CYCLIC NUCLEOTIDE-GATED ION CHANNELs 14 and 16 Promote Tolerance to Heat and Chilling in Rice[1][OPEN]

Yongmei Cui,[a,2] Shan Lu,[a,2] Zhan Li,[b] Jiawen Cheng,[a] Peng Hu,[a] Tianquan Zhu,[a] Xiang Wang,[a] Mei Jin,[c] Xinxue Wang,[a] Luqi Li,[a] Shuying Huang,[a] Baohong Zou,[a,3] and Jian Hua[a,b,3,4]

[a]The State Key Laboratory of Crop Genetics and Germplasm Enhancement, Nanjing Agricultural University, Nanjing 210095, China
[b]Plant Biology Section, School of Integrated Plant Science, Cornell University, Ithaca, New York 14853
[c]National Experimental Teaching Center for Plant Production, Nanjing Agricultural University, Nanjing 210095, China

ORCID ID: 0000-0002-3777-3344 (J.H.).

Calcium signaling has been postulated to be critical for both heat and chilling tolerance in plants, but its molecular mechanisms are not fully understood. Here, we investigated the function of two closely related cyclic nucleotide-gated ion channel (CNGC) proteins, OsCNGC14 and OsCNGC16, in temperature-stress tolerance in rice (*Oryza sativa*) by examining their loss-of-function mutants generated by genome editing. Under both heat and chilling stress, both the *cngc14* and *cngc16* mutants displayed reduced survival rates, higher accumulation levels of hydrogen peroxide, and increased cell death. In the *cngc16* mutant, the extent to which some genes were induced and repressed in response to heat stress was altered and some *Heat Shock factor* (*HSF*) and *Heat Shock Protein* (*HSP*) genes were slightly more induced compared to the wild type. Furthermore, the loss of either *OsCNGC14* or *OsCNGC16* reduced or abolished cytosolic calcium signals induced by either heat or chilling stress. Therefore, *OsCNGC14* and *OsCNGC16* are required for heat and chilling tolerance and are modulators of calcium signals in response to temperature stress. In addition, loss of their homologs *AtCNGC2* and *AtCNGC4* in Arabidopsis (*Arabidopsis thaliana*) also led to compromised tolerance of low temperature. Thus, this study indicates a critical role of *CNGC* genes in both chilling and heat tolerance in plants, suggesting a potential overlap in calcium signaling in response to high- and low-temperature stress.

Plant growth and development is highly regulated by environmental factors including temperature. Extreme temperatures cause an array of biochemical, physiological, and morphological changes in plants and often negatively impact plant productivity (Hatfield and Prueger, 2015; Liu et al., 2016; Leeggangers et al., 2017). Developing plant varieties that are tolerant to high and low temperatures is a challenge for researchers in plant biology and agriculture (Atkinson and Porter, 1996). Both high and low temperatures induce complex responses in plants, some of which may provide protection against stresses and damage (Wada et al., 1990; Murakami et al., 2000). Primary temperature sensing is thought to occur on membranes potentially through membrane fluidity and membrane-localized channels or receptors (Murata and Los, 1997). Sensing is followed by the generation of secondary messengers, including Ca^{2+} and reactive oxygen species (ROS; Yan et al., 2006). Both heat and cold induce transient Ca^{2+} influx into the cell cytoplasm (Finka et al., 2012; Ma et al., 2015), and repeated cold treatment can induce repetitive Ca^{2+} transients (Krebs et al., 2012). ROS, at moderate amounts, may induce ROS scavengers and other protective mechanisms for stress tolerance (Prasad et al., 1994). Excess ROS cause oxidative damage to cells, leading to growth defects or initiation of programmed cell death (Mittler, 2002). The secondary Ca^{2+} signals and ROS can initiate another cascade of signaling events, which may have different signaling and physiological consequences depending on the primary stimuli (Zhang et al., 2019). In heat signaling, a transient increase of Ca^{2+} is thought to promote expression of the calmodulin (*CaM*) genes (Liu et al., 2003), and CaM can regulate the activities of CaM-binding protein kinase or heat-activated mitogen-activated protein kinase (Nguyen and Shiozaki, 1999;

[1]This work was supported by the National Science Foundation of China (grant nos. 31700223 to S.L. and 31670269 to J.H.), Fundamental Research Funds for the Central Universities (grant nos. KJQN201807 to S.L., and KYZ201813 to J.H.), open funds of the State Key Laboratory of Plant Physiology and Biochemistry (grant no. SKLPPBKF1501 to B.Z.), the Jiangsu Collaborative Innovation Center for Modern Crop Production, and the Cyrus Tang Innovation Center for Seed Industry.

[2]These authors contributed equally to the article.

[3]Senior authors.

[4]Author for contact: jh299@cornell.edu.

The author responsible for distribution of materials integral to the findings presented in this article in accordance with the policy described in the Instructions for Authors (www.plantphysiol.org) is: Jian Hua (jh299@cornell.edu).

J.H., S.L., Y.C., and B.Z. designed the research; Y.C., S.L., Z.L., P.H., T.Z., Xia.W., M.J., Xin.W., L.L., and S.H. performed the experiments; Y.C., J.H., J.C., S.L., and B.Z. analyzed the data; and Y.C. and J.H. wrote the manuscript with input from other authors.

[OPEN]Articles can be viewed without a subscription.
www.plantphysiol.org/cgi/doi/10.1104/pp.20.00591

Liu et al., 2008). The activated kinases phosphorylate heat shock factors (HSFs) and promote the expression of *Heat Shock Proteins* (*HSPs*), leading to the heat shock response (HSR) and the onset of thermotolerance (Saidi et al., 2011). HSPs are chaperone proteins important for controlling damage from denatured and aggregated proteins caused by heat (Ohama et al., 2017). HSPs can be induced by both the HSR and an active unfolded protein response in the endoplasmic reticulum (ER); the unfolded protein response can stabilize, renature, and degrade unfolded proteins to enhance survival under heat (Fragkostefanakis et al., 2016; Rieu et al., 2017). In cold signaling, it is thought that cold sensors located on membranes trigger Ca^{2+} influx, leading to activation of kinases that ultimately modulate the activity and abundance of Inducer of C-repeat Binding Factor (CBF) Expression1 (ICE1). In Arabidopsis (*Arabdopsis thaliana*), AtICE1 regulates the expression of *CBF* genes as well as other cold-responsive transcription factors, resulting in increased freezing tolerance (Stockinger et al., 1997; Liu et al., 1998; Zhang et al., 2019). In rice (*Oryza sativa*), OsICE1 is phosphorylated by mitogen-activated protein kinase3, resulting in a higher protein stability, which leads to the accumulation of trehalose and improved chilling tolerance (Zhang et al., 2017).

Cyclic nucleotide-gated ion channels (CNGCs) are nonselective, ligand-gated cation channels present across eukaryotes (Liu et al., 2018). In plants, CNGCs are found to be involved in diverse processes and their functions are thought to result from their involvement in calcium influx. Arabidopsis has 20 CNGCs, which have been implicated in regulating plant growth and development, biotic/abiotic stress responses, and ion homeostasis (DeFalco et al., 2016). In growth and development, *AtCNGC1*, *AtCNGC2*, and *AtCNGC10* are shown to modulate multiple processes (Chan et al., 2003; Ma et al., 2006; Borsics et al., 2007); *AtCNGC5*, *AtCNGC6*, *AtCNGC9*, and *AtCNGC14* are required for growth of root hairs (Brost et al., 2019; Tan et al., 2019); *AtCNGC7*, *AtCNGC8*, and *AtCNGC18* are essential for pollen germination and male fertility (Pan et al., 2019); and *AtCNGC17* participates in protoplast expansion (Ladwig et al., 2015). In biotic stress responses, *AtCNGC2*, *AtCNGC4*, *AtCNGC11*, and *AtCNGC12* play a role in pathogen response, whereas *AtCNGC19* regulates defense against *Spodoptera* spp. herbivory (Yoshioka et al., 2006; Chin et al., 2013; Meena et al., 2019). In abiotic stress responses, *AtCNGC3*, *AtCNGC10*, *AtCNGC19*, and *AtCNGC20* are involved in adaptation to salt stress (Gobert et al., 2006; Guo et al., 2008; Kugler et al., 2009), whereas *AtCNGC2*, *AtCNGC4*, *AtCNGC6*, and *AtCNGC16* in Arabidopsis have been implicated in heat-stress adaptation (Finka et al., 2012; Gao et al., 2012; Tunc-Ozdemir et al., 2013). Disruption of *AtCNGC2* and *AtCNGC4* in Arabidopsis and its putative ortholog *PpCNGCb* in moss (*Physcomitrella patens*) resulted in enhanced acquired thermotolerance in seedlings, and the loss of function of *PpCNGCb* in moss was accompanied by a higher HSR and higher Ca^{2+} influx than in the wild type (Finka et al., 2012). Interestingly, deficiency in *AtCNGC2* resulted in more heat susceptibility at the reproductive stage in contrast to the enhanced heat tolerance at seedling stage (Katano et al., 2018), suggesting a developmental stage-dependent function of CNGCs in stress tolerance. *AtCNGC6* was shown to be activated by cytosolic cAMP and to promote expression of *HSP* genes and acquired thermotolerance (Gao et al., 2012). *AtCNGC16* plays an essential function in pollen fertility under heat stress (Tunc-Ozdemir et al., 2013). The diverse function of CNGCs is thought to result from their functions in modulating calcium influx. *AtCNGC2* is shown to affect Ca^{2+} influx into leaf cells to prevent Ca^{2+}-induced hydrogen peroxide (H_2O_2) accumulation, cell death, and leaf senescence (Wang et al., 2017). In rice, 16 CNGC members have been identified (Nawaz et al., 2014), but only two are functionally characterized. The *OsCNGC13* gene is a maternal sporophytic factor that functions in regulating rice seed setting and the *OsCNGC9* gene was recently shown to mediate pathogen-associated molecular pattern-induced Ca^{2+} influx in plant immunity (Xu et al., 2017; Wang et al., 2019).

In this study, we found that the rice *OsCNGC14* and *OsCNGC16* genes play critical roles in heat tolerance as well as low-temperature tolerance. In addition, they affect Ca^{2+} influx to the cytosol in response to heat or cold treatments. Our study thus provides evidence for the role of CNGC proteins in calcium regulation and uncovers a further function of CNGC proteins in chilling and freezing tolerance in addition to their known roles in heat tolerance in plants.

RESULTS

Generation of the *cngc14* and *cngc16* Mutants

Given that *AtCNGC2*, *AtCNGC4*, and *PpCNGCb* play key roles in thermotolerance in Arabidopsis and moss (Finka et al., 2012), we investigated the roles of their rice homologs in temperature-stress tolerance. The complementary DNA (cDNA) sequences of these three genes were used to Blast search the rice genome sequences, and their most similar genes in rice were identified as *OsCNGC14*, *OsCNGC15*, and *OsCNGC16* (Supplemental Fig. S1). Because we were not able to generate mutants in *OsCNGC15* as in *OsCNGC14* and *OsCNGC16*, we focused our study on the latter two genes. We first determined the subcellular localization of these two rice CNGC proteins by fusing them with GFP. Transient expression of these fusion proteins in *Nicotiana benthamiana* revealed that OsCNGC14 and OsCNGC16 are both localized to the plasma membrane (Supplemental Fig. S2). A search of the Rice Expression Profile Database showed that the *OsCNGC14* and *OsCNGC16* genes are expressed in most organs, including leaves, stems, inflorescence, and reproductive organs, and *OsCNGC14* has a much higher expression level than *OsCNGC16* in general (Supplemental Fig. S3,

A and B). We assessed the expression of these genes in response to heat and cold treatments by reverse transcription quantitative PCR (RT-qPCR). The *OsCNGC14* gene was induced by 42°C treatment to a maximum of 5.6-fold at 3 h, dropped at 6 h, and came down to almost the basal level at 9 h of heat treatment. The *OsCNGC16* gene was induced to a maximum of 3.4-fold at 3 h and decreased to almost the basal level at 6 h of heat treatment (Supplemental Fig. S4A). In response to the 6°C chilling treatment, the expression of *OsCNGC14* was increased by 1.6-fold at 1 h and dropped to the basal level at 3 h, whereas expression of the *OsCNGC16* gene reached a maximum of 3.1-fold at 6 h compared to the basal level and dropped to basal level at 9 h (Supplemental Fig. S4B).

To assess the function of *OsCNGC14* and *OsCNGC16* genes in rice, we generated their mutants in the cv Nipponbare background via CRISPR/Cas9 technology (Xing et al., 2014). Homozygous mutants were identified among the T_0 population by sequencing the region around the CRISPR target sites. Three *OsCNGC14* mutants (*cngc14-1*, *cngc14-2*, and *cngc14-3*) and three *OsCNGC16* mutants (*cngc16-1*, *cngc16-2*, and *cngc16-3*) were obtained. The *cngc14-1* mutant contained an 8-bp deletion (193–200 bp) and a 1-bp deletion at 224 bp relative to the translation start site, leading to a predicted 3-amino acid deletion (amino acids 65–67) in its predicted coding protein (Fig. 1, A and B). The *cngc14-2* mutant contained a 25-bp deletion (176–200 bp) and a 1-bp insertion at 225 bp, leading to a predicted 8-amino acid deletion (amino acids 59–66; Fig. 1, A and B). The *cngc14-3* mutant contained a 28-bp deletion (197–224 bp), which is predicted to produce an altered protein sequence starting at amino acid 66 and a stop codon at amino acid 83 (Fig. 1, A and B). The *cngc16-1* mutant contained 1-bp insertions at 585 and 718 bp, which are predicted to produce an altered protein sequence starting at amino acid 195 and a stop codon at amino acid 262 (Fig. 1, C and D). The *cngc16-2* mutant contained a 3-bp deletion (586–588 bp) and a 1-bp insertion at 718 bp, causing a predicted 1-amino acid deletion at position 196 and a reading frame shift after position 240 (Fig. 1, C and D). The *cngc16-3* contained a 7-bp deletion (585–591 bp), a 1-bp insertion at 718 bp, and a 1-bp substitution at 719 bp, which is predicted to produce an altered protein sequence starting at amino acid 196 and a stop codon at amino acid 204 (Fig. 1, C and D).

We assayed the mRNA expression of *OsCNGC14* and *OsCNGC16* in their respective mutants by semiquantitative RT-PCR using primers spanning the CRISPR target sites. The transcripts of *OsCNGC14* were found to be greatly reduced in all three *cngc14* mutant alleles compared to the wild type, with *cngc14-3* having the lowest expression (Fig. 1B; Supplemental Fig. S5A). The transcripts of *OsCNGC16* were also greatly reduced in all three *cngc16* mutant alleles compared to the wild type with *cngc16-3* having the lowest expression (Fig. 1D; Supplemental Fig. S5B). The drastically reduced expression of *OsCNGC14* or *OsCNGC16* associated with some alleles is likely due to nonsense-mediated mRNA degradation. Taken together, *cngc14-1* and *cngc14-2* are likely reduction-of-function mutants, because lower levels of mRNA are produced and small deletions are present in the predicted proteins. The *cngc14-3* allele and all three *cngc16* alleles are most likely loss-of-function mutants, because the amounts of mRNA present are lower than in the wild type and the predicted proteins have large truncations and therefore are likely nonfunctional (Fig. 1, B and D).

OsCNGC14 and *OsCNGC16* Promote Thermotolerance in Rice at Seedling Stage

To determine whether *OsCNGC14* and *OsCNGC16* play roles in heat tolerance, the rice *cngc14* and *cngc16* mutants were subjected to a heat treatment. None of these *cngc14* and *cngc16* mutant plants had any overt abnormalities or defects when grown under normal conditions. Two-week-old seedlings were treated at 48°C for 48 h, and the loss of green color and survival rates were analyzed after a 2-week recovery growth at 26°C. The *cngc14* and *cngc16* mutants had more withered and yellower leaves compared to the wild-type cv Nipponbare plants (Fig. 2A). The mutants also had lower survival rates than the wild type. The *cngc14-1*, *cngc14-2*, *cngc14-3*, *cngc16-1*, *cngc16-2*, and *cngc16-3* had survival rates of 66%, 51%, 24%, 23%, 23%, and 30%, respectively, each of which was significantly lower than the rate of 70% for the wild type except that of *cngc14-1* (Fig. 2B). The difference in survival rates among *cngc14-1*, *cngc14-2*, and *cngc14-3* is consistent with the prediction that *cngc14-3* is a loss-of-function allele and the other two are reduction-of-function alleles. We further tested seedling tolerance by longer exposure (72 h) to a moderate heat of 43°C. After the heat treatment, the *cngc14* and *cngc16* mutant plants had severely wrinkled and rough leaves and the *cngc16* mutant developed necrotic spots on leaves, whereas the wild type was only slightly wrinkled at the leaf tip (Supplemental Fig. S6A). In addition, ion leakage in leaves, an indicator of membrane damage, was dramatically increased in the *cngc14-2* mutant and three *cngc16* mutants compared with wild-type plants after heat treatment but not in plants without heat treatment (Fig. 2C). Furthermore, whereas before heat treatment the mutants had low accumulation of H_2O_2, similar to that of the wild type, a higher accumulation relative to the wild type was observed after heat treatment, as assayed by staining with 3,3′-diaminobenzidine (DAB; Fig. 2D). Heat also induced moderate cell death in the wild type, as indicated by trypan blue staining, and the *cngc14* and *cngc16* mutants exhibited more cell death compared with the wild-type plants after heat treatment but not without heat treatment (Fig. 2E). These results indicate that *OsCNGC14* and *OsCNGC16* positively contribute to heat tolerance in rice and that loss or reduction of their function leads to higher heat susceptibility

associated with higher accumulation of H_2O_2 and cell damage.

OsCNGC14 and *OsCNGC16* Impact Cytosolic Calcium Increase in Response to Heat Treatment

Because heat shock induces a transient increase in cytosolic Ca^{2+} (Saidi et al., 2009; Zheng et al., 2012), we investigated whether *OsCNGC14* and *OsCNGC16* affect the production of such a calcium signal. The cytosolic calcium concentration was detected by a nuclear export signal (NES) version of the calcium sensor Yellow Cameleon 3.6 (YC3.6) based on fluorescence resonance energy transfer (FRET; Krebs et al., 2012). This NES-YC3.6 reporter was introduced into the *cngc14-2* and *cngc16-1* mutants by crossing, and isogenic lines of the wild type and the *cngc* mutants with the same reporter gene were generated (Supplemental Fig. S7, A–C). Calcium concentrations, measured by the FRET signals (cpVenus/cyan fluorescent protein), were analyzed in stomatal cells where YC3.6 has a strong expression (Supplemental Fig. S7, D–G). Under normal growth conditions, no significant difference was observed

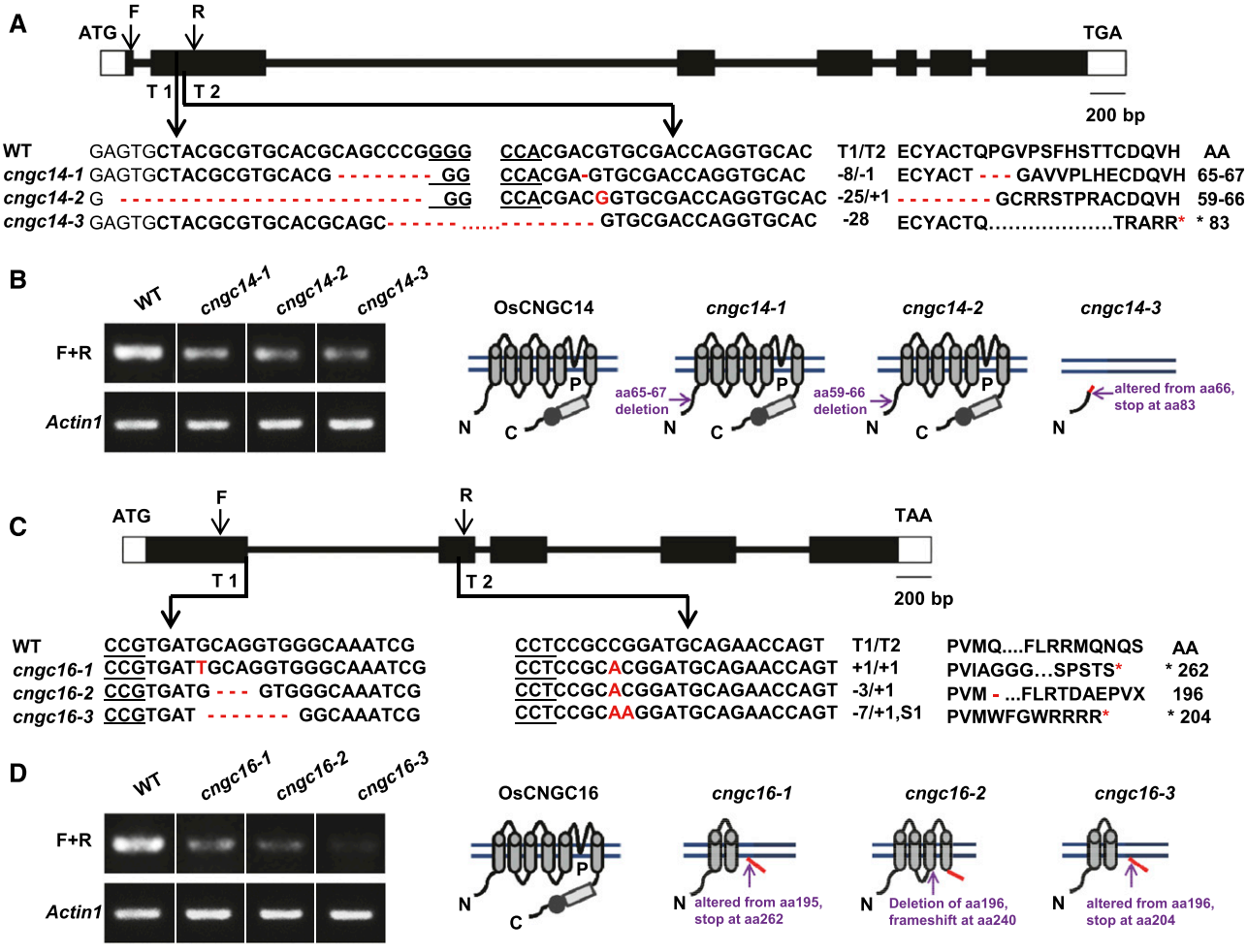

Figure 1. Mutants of *OsCNGC14* and *OsCNGC16* generated by CRISPR/Cas9 technology. Diagram of the genomic sequences (A and C) and predicted protein structures (B and D) of the wild type (WT) and mutants of Os*CNGC14* (A and B) and *OsCNGC16* (C and D). A and C, Diagrams of the genomic DNA, with exons, introns, and untranslated regions indicated by black boxes, lines between boxes, and white boxes, respectively. Below the diagrams are sequence alignments between the mutants and wild type, with genomic sequences on the left and protein sequence on the right. Minus (−) and plus (+) signs and the letter S indicate the number of nucleotides deleted, inserted, and substituted, respectively, within the CRISPR/Cas9 target sequences T1 and T2. The asterisk indicates a stop codon generated. F, Forward primers; R, reverse primers. B and D, RNA expression and predicted protein structures of OsCNGC14 (B) and OsCNGC16 (D) in the wild type and the *cngc* mutants. On the left are products of semi-quantitative RT-PCR of *OsCNGC14* and *OsCNGC16* in their respective mutants and the wild type. *Actin1* was used as a control gene. On the right are diagrams of predicted protein structure in the wild type and different mutant alleles. For each structure, transmembrane helices are indicated by cylinders, the cyclic nucleotide binding domain by a rectangle, and the calmodulin-binding domain by a solid circle. Locations of amino acid alterations are indicated by arrows. Red lines indicate altered sequences from frameshift.

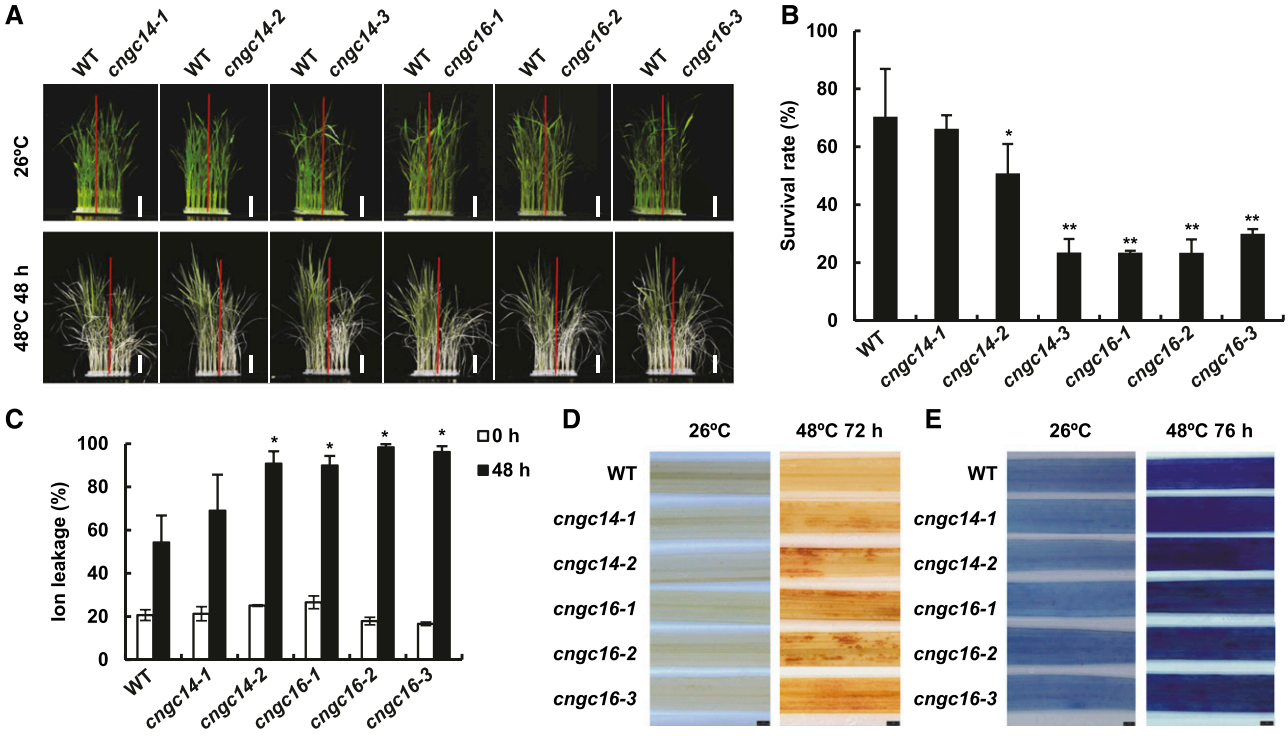

Figure 2. Mutants of *OsCNGC14* and *OsCNGC16* are heat susceptible at seedling stage. A, Morphological phenotypes of the wild type (WT), *cngc14*, and *cngc16* seedlings before and after heat treatment. Seedlings were hydroponically grown at 26°C for 2 weeks and then treated at 48°C for 48 h followed by a recovery at 26°C for 2 weeks. Plants were photographed after the recovery. Scale bars = 2 cm. B, Survival rates for the *cngc14* and *cngc16* mutants shown in A. Shown are the means ± SD for three biological replicates ($n = 48$ for each replicate). At least three independent experiments were carried out with similar results. C, Cellular ion leakage with or without 48°C treatment for 48 h in the third leaves of 2-week-old seedlings grown hydroponically at 26°C. Shown are means ± SD from four biological replicates, with 12 plants for each line. Asterisks indicate significant difference by Students *t* test (*$P < 0.05$ and **$P < 0.01$). D and E, H_2O_2 accumulation detected by DAB staining (D) and cell death detected by trypan blue staining (E) in the third leaves of 3-week-old seedlings grown in the soil before and after treatment at 48°C for 72 and 76 h, respectively ($n = 15$). Scale bars = 1 mm.

between wild-type and *cngc14* or *cngc16* mutants in cytosolic Ca^{2+} levels (Supplemental Fig. S7H). Drastic differences in Ca^{2+} levels were observed when heat shock was applied to leaves. In response to heat treatment, the cytosolic Ca^{2+} concentration rose quickly in the wild type, reached the maximum at 15 s (seconds), and declined sharply (Fig. 3, A and B; Supplemental Movie S1). This "spike and shoulder"-shaped cytosolic Ca^{2+} was consistent with earlier reports in Arabidopsis and rice (Behera et al., 2015). Each of the subsequent heat treatments at the frequency of once every minute induced a calcium spike with a similar shape to the first spike (at least up to the seventh treatment; Fig. 3, A and B; Supplemental Movie S1). The *cngc14-2* mutant displayed a significant decrease in cytosolic calcium spike after the first heat treatment, and it showed weaker spikes with subsequent treatments compared to the wild type (Fig. 3, A and C; Supplemental Movie S2). This indicates that Ca^{2+} kinetics was milder in the *cngc14-2* mutant compared to the wild type. The *cngc16-1* mutant exhibited a much stronger defect in calcium signal compared to the *cngc14-2* mutant. The heat-induced transient increase of cytosolic Ca^{2+} was largely abolished in the *cngc16-1* mutant (Fig. 3, A and D; Supplemental Movie S3). The maximal changes in FRET signals (apparent FRET efficiency/apparent rest FRET efficiency $[\Delta E_{app}/E_{apprest}]$) in *cngc14-2* and *cngc16-1* were 0.10 ± 0.09 and 0.02 ± 0.07, respectively, which were significantly lower than the signal 0.33 ± 0.15 seen in the wild type for the first peak (Fig. 3, E and F). In conclusion, *OsCNGC14* and *OsCNGC16* are positive modulators of heat-induced increase of cytosolic calcium. It remains to be determined whether the lesser severity of defects in the *cngc14-2* mutant compared to the *cngc16-1* mutant is due to the reduction-of-function nature of the *cngc14-2* allele.

Transcriptome Analysis of the *cngc16* Mutant

To further investigate how CNGCs regulate heat tolerance in rice, we carried out RNA sequencing (RNA-Seq) to profile transcriptomes of the wild type and the *cngc16-3* mutant. Rice plants grown at 26°C for 2 weeks were heat treated at 42°C, and RNAs were extracted from leaf tissues at 0, 3, and 24 h after

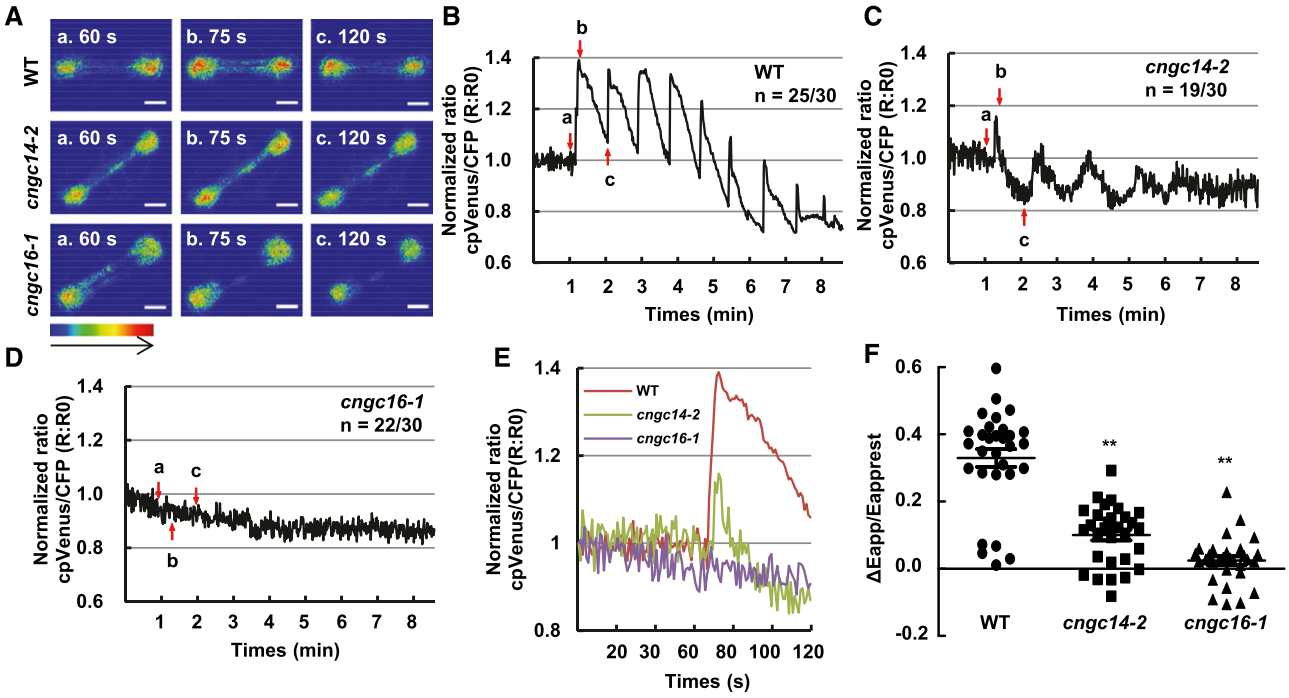

Figure 3. Heat-induced cytosolic Ca^{2+} changes in guard cells of *cngc14* and *cngc16* mutants. A, Emission images of cytosolic Ca^{2+} in the stomatal cells from leaves of wild-type (WT), *cngc14-2*, and *cngc16-1* 10-d-old seedlings expressing NES-YC3.6. Shown are representative images before heat shock treatment (60 s) and after heat shock buffer administration (75 and 120 s). The representative image of relative cytosolic Ca^{2+} is represented as the emission fluorescence ratio and scaled by a pseudo-color bar (bottom). Scale bars = 50 μm. B to D, Normalized cytosolic Ca^{2+} FRET ratio in stomatal cells. The luminescence was recorded at 1-s intervals. Shown are representative images of calcium signals in stomatal cells of the wild type, *cngc14-2*, and *cngc16-1*. Lowercase letters refer to the time points at which these ratio images were taken in A. A total of 30 stomatal cells (one leaf/plant, 1–2 stomatal cells/leaf) in the third leaves from at least 15 different seedlings were measured. The two numbers underneath each genotype indicate the number of cells with the representative calcium pattern versus the number of total cells analyzed. E, Representative traces of calcium signals from the wild type and mutants are shown together. F, Scatter plots of the heat-induced changes in cytosolic calcium ($\Delta E_{app}/E_{apprest}$) in wild type, *cngc14-2*, and *cngc16-1*, as shown in B to D. The Δ cytosolic Ca^{2+} indicates the changes between the $[Ca^{2+}]^{peak}$ and $[Ca^{2+}]^{rest}$. Data are from all 30 cells that were monitored for each genotype. Asterisks indicate significant difference by Student's *t* test ($^{**}P < 0.01$).

heat treatment. Differentially expressed genes (DEGs) among samples were defined by a fold change of $|\log_2| \geq 1$ and a false discovery rate (FDR) $\leq$0.01. Overall, high correlation values were observed for three biological repeats for each genotype and time point combination ($r \geq 0.92$; Supplemental Fig. S8A), indicating a good reproducibility of the samples. Principal component analysis (PCA) also revealed that the biological repeats are clustered together (Supplemental Fig. S8B). Interestingly, the 0-h samples of the wild type and the *cngc16-3* mutant were closely clustered, indicating that without heat treatment, the wild type and the mutant are similar in RNA expression. PC1 divided the 0-h samples from the 3- and 24-h samples, indicating that temperature, and not genotype, has the largest impact on transcriptomes. PC2 separated the 0-, 3-, and 24-h samples and also showed that RNA expression at 3 h is more different from that at 0 and 24 h. The genotype difference was less pronounced than the heat and time differences, indicating that the wild type and the mutant are in general similar in transcriptome responses before and after heat treatment. In addition, PC1 distribution revealed that the *cngc16-3* mutant at 3 and 24 h is more distant from the wild type or *cngc16-3* at 0 h compared to the wild type at the corresponding 3- and 24-h time points (Supplemental Fig. S8B), suggesting that there are more changes in the *cngc16-3* mutant than in the wild type in response to heat.

Comparisons of DEGs between the wild type and the *cngc16-3* mutant, as well as between heat treatment and non-heat treatment, also indicated that the transcriptome responses to heat were similar in the wild type and the mutant. At 0, 3, and 24 h, a total of 150, 404, and 510 genes, respectively, had increased expression, whereas a total of 84, 44, and 576 genes had decreased expression, in the *cngc16-3* mutant compared to the wild type (Supplemental Table S1). No significant gene ontology (GO) enrichment was observed for these DEGs between the *cngc16-3* mutant and the wild type at 0, 3, or 24 h of heat treatment. When comparing heat treatment (3 or 24 h) to non-heat treatment (0 h), a larger number of DEGs (in thousands) was found for both the

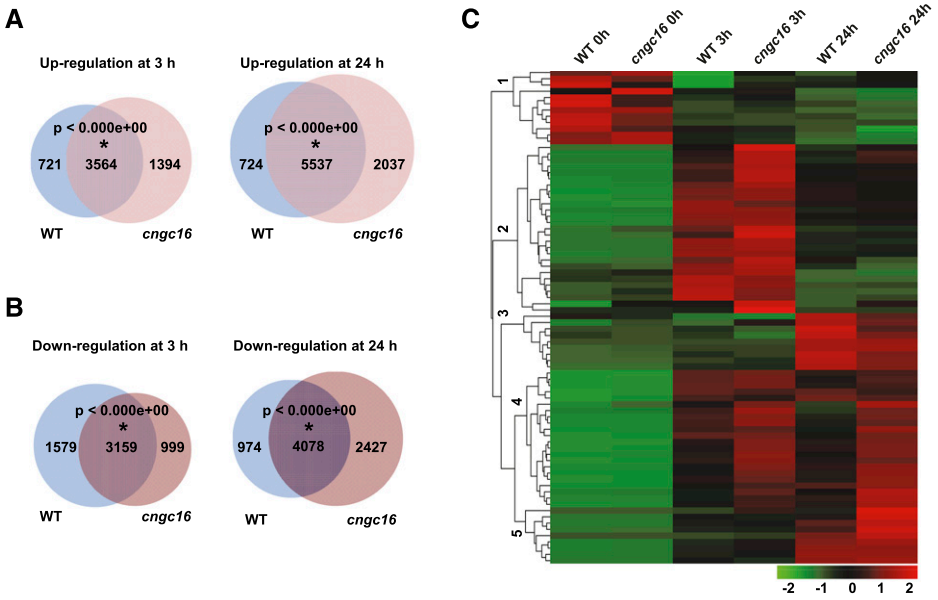

Figure 4. RNA-Seq analysis of the *cngc16* mutant. A and B, Venn diagrams of heat-induced (A) and heat-repressed (B) genes in the wild type (WT) and *cngc16-3*. Two-week-old seedlings were treated at 42°C for 0, 3, and 24 h for RNA-Seq analysis. Expression at 3 or 24 h was compared to that at 0 h, and DEGs were defined by $\log_2$ fold change ≥ 1 or ≤ -1, and FDR < 0.01. The DEGs were used to draw the Venn diagram via tools accessed at http://bioinfogp.cnb.csic.es/tools/venny/. Statistical significance ($P < 0.01$) of the overlap is indicated by an asterisk, calculated using the online program http://nemates.org/MA/progs/overlap_stats.html. C, Heatmap representation of expression levels of DEGs of *HSF* and *HSP* genes at 0, 3, and 24 h after 42°C heat treatment in wild type and the rice *cngc16-3* mutant.

wild type and the mutant (Fig. 4, A and B; Supplemental Tables S2 and S3). A Venn diagram showed significant overlap between the wild type and the *cngc16-3* mutant in both up- and down-regulated DEGs at 3 and 24 h (Fig. 4, A and B). This suggests that the mutant is not drastically different from the wild type before or after heat treatment. GO-term analysis also revealed that the wild type and the mutant had almost identically enriched GO terms in DEGs at 3 h (or 24 h) versus 0 h (Supplemental Fig. S9, A–D). Heat-induced DEGs in the wild type and the *cngc16-3* mutant were both enriched in GO terms including "response to salt stress," "response to reactive oxygen species," "cellular response to heat," "response to cold," and "chaperone-mediated protein folding" (Supplemental Fig. S9, A and B). The heat-repressed DEGs in the wild type and the *cngc16-3* mutant were enriched in GO terms related to growth and development, such as "plant-type cell wall biogenesis," "sterol biosynthetic process," "metal ion transport," and "cellular amino acid biosynthetic process" (Supplemental Fig. S9, C and D).

We further examined DEGs between the wild type and *cngc16-3* mutant at 3 or 24 h to determine whether they represented any unique pathways. GO-term analysis did not reveal any enriched terms; however, these DEGs have significant overlaps with DEGs of heat versus nonheat in the wild type. Among the 404 upregulated DEGs in the *cngc16-3* mutant compared to the wild type at 3 h, 105 were heat induced and 94 were heat repressed in the wild type (Supplemental Fig. S10A). This suggests that heat responses (induction or repression) are larger for some and smaller for other genes in the *cngc16-3* mutant compared to the wild type (Supplemental Fig. S10A). This was similarly observed for DEGs between the wild type and the mutant at 24 h, that is, they have significant overlaps with heat-induced or heat-repressed genes in the wild type, and they are more responsive or less responsive to heat in the mutant compared to the wild type (Supplemental Fig. S10, C and D). Taken together, there was no qualitative difference between the wild type and the *cngc16-3* mutant in terms of heat response at the transcriptome level, but the extent of responses for some genes differs between the mutant and the wild type.

Because the Arabidopsis *cngc2* mutant had increased expression of *HSP* genes compared to the wild type in response to heat (Finka et al., 2012), we examined the expression of *HSF* and *HSP* genes in the *cngc16* mutant. Among the 100 *HSF* and *HSP* genes in rice, 79 were identified as DEGs ($\log_2$ fold change ≥ 1 or ≤ -1 and FDR < 0.01) using the normalized expression data in this study, which is almost exclusively due to their induction by heat (Supplemental Table S4). Among all of these *HSF* and *HSP* DEGs, only two displayed a significant expression difference between the mutant and the wild type at 24 h, and none were DEGs at 0 or 3 h (Supplemental Table S4). This indicates that expression levels of *HSF* and *HSP* genes in general are similar between the mutant and the wild type (<2-fold difference) with or without heat treatment. Cluster analyses of these 79 DEGs of *HSF* and *HSP* genes by their expression revealed five coexpression groups (Fig. 4C). Heatmap analysis showed that genes in groups 1 and 3 had lower relative expression levels in the *cngc16-3* mutant compared to the wild type at 0 and 24 h, respectively (Fig. 4C; Supplemental Table S4). By contrast, genes in groups 2, 4, and 5 had higher induction by heat in the *cngc16-3* mutant compared to the wild type at 3 and/or 24 h (Fig. 4C; Supplemental Table S4). These results indicate that the rice *cngc16-3* mutant has slightly increased induction of primarily *HSF* and *HSP* genes after heat treatment at 3 or 24 h. *cngc16-3* does not have an attenuated induction of *HSFs* and *HSPs* during heat shock, which is in contrast to the enhanced induction observed in the

Arabidopsis *cngc6* mutant but similar to induction observed in the *cngc16* mutants (Gao et al., 2012; Tunc-Ozdemir et al., 2013).

OsCNGC14 and *OsCNGC16* Enhance Chilling Tolerance in Rice at Seedling Stage

CNGCs have not been associated with cold responses in plants. The drastic calcium signal defect of the rice *cngc14* and *cngc16* mutants in response to heat promoted us to analyze their function in cold tolerance, where calcium signal is also thought to be a secondary messenger. The *cngc14* and *cngc16* mutants, as well as the wild type, were subjected to a chilling (cold but above freezing) treatment of 6°C for 72 h performed on 2-week-old seedlings followed by a 2-week recovery growth period at 26°C. Each of the mutants analyzed, namely *cngc14-1*, *cngc14-2*, *cngc14-3*, *cngc16-1*, *cngc16-2*, and *cngc16-3*, exhibited reduced growth and yielded yellower leaves after chilling treatment compared to the wild-type plants (Fig. 5A; Supplemental Fig. S6B). In addition, all mutants had lower survival rates from chilling treatment compared to the wild type (Fig. 5B). *cngc14-1*, *cngc14-2*, *cngc14-3*, *cngc16-1*, *cngc16-2*, and *cngc16-3* exhibited survival rates of 43%, 36%, 22%, 28%, 17%, and 27%, respectively, significantly lower than the rate of 65% for the wild type (Fig. 5B).

We subsequently examined the response to chilling stress in the *cngc14* and *cngc16* mutants at the cellular level. Chilling induced increased ion leakage in leaf cells of the wild-type plants due to damage to cellular membranes (Fig. 5C). The *cngc14* and *cngc16* mutant plants all had significantly increased ion leakage in leaves compared to the wild-type plants at 72 h after chilling, whereas they did not differ from the wild type before chilling treatment (Fig. 5C). Chilling induced accumulation of ROS, including H_2O_2, as assayed by DAB staining (Fig. 5D). Both the *cngc14* and *cngc16* mutants accumulated more H_2O_2 than the wild-type plants after 96 h of chilling treatment, whereas both the mutants and the wild type had low amounts of H_2O_2 before chilling treatment (Fig. 5D). Chilling also

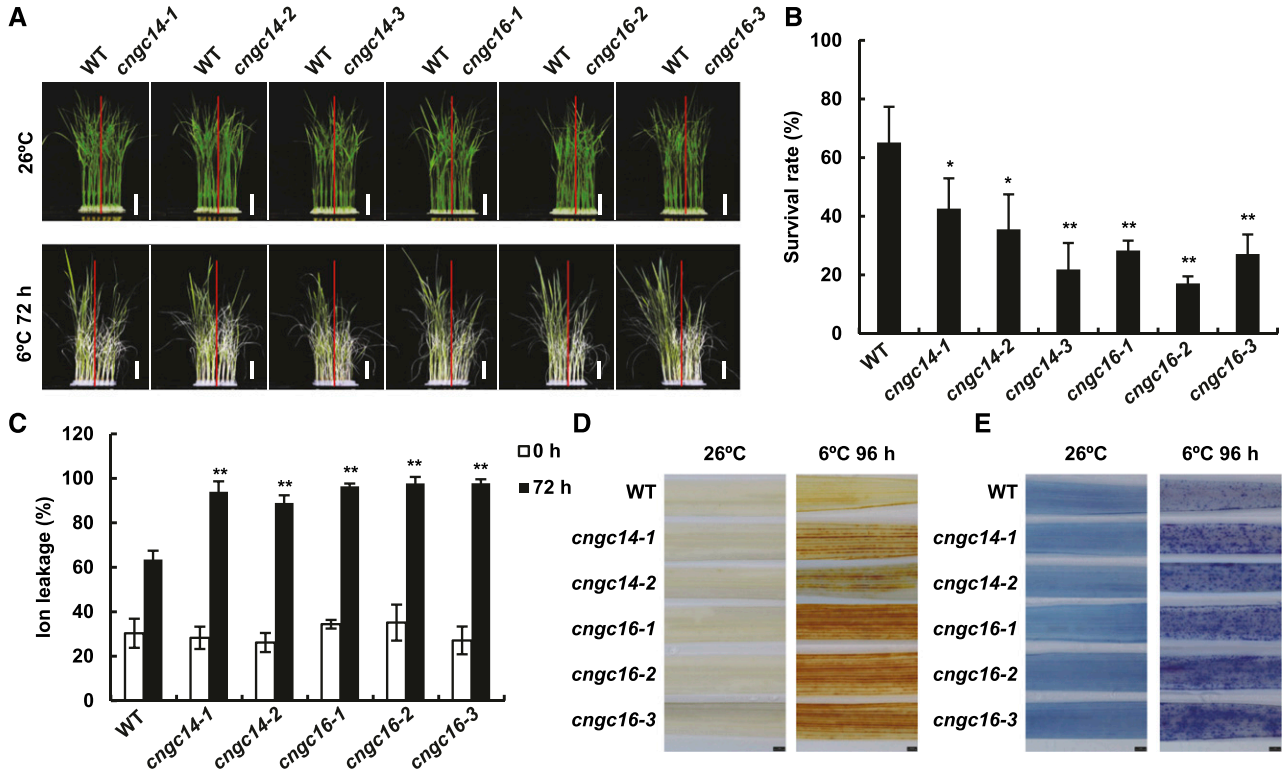

Figure 5. Mutants of *OsCNGC14* and *OsCNGC16* are chilling susceptible at seedling stage. A, Morphological phenotypes of wild-type (WT), *cngc14*, and *cngc16* seedlings before and after chilling treatment. Seedlings were hydroponically grown at 26°C for 2 weeks and then treated at 6°C for 72 h followed by recovery at 26°C for 2 weeks. Plants were photographed after the recovery. Scale bars = 2 cm. B, Survival rates of the *cngc14* and *cngc16* mutants after chilling treatment as in A. The data are the means ± SD of three biological replicates ($n = 48$ for each replicate). Three independent experiments were carried out with similar results. C, Cellular ion leakage with or without 6°C treatment for 72 h in the third leaves of 2-week-old seedlings grown hydroponically at 26°C. Data represent means ± SD from four biological replicates with 12 plants for each line. Asterisks indicate significant difference by Student's *t* test (*$P < 0.05$ and **$P < 0.01$). D and E, H_2O_2 accumulation detected by DAB staining (D) and cell death detected by trypan blue staining (E) in the third leaves of 3-week-old seedlings grown in soil before and after a treatment of 6°C for 96 h ($n = 15$). Scale bars = 1 mm.

induced cell death in the wild-type plants, as indicated by trypan blue staining (Fig. 5E). The *cngc14* and *cngc16* mutants exhibited more cell death compared to the wild type after 96 h of chilling treatment, whereas they did not show increased cell death before chilling (Fig. 5E). Taken together, these results indicate that *OsCNGC14* and *OsCNGC16* are important for chilling tolerance in rice and that the loss or reduction of their function leads to reduced chilling tolerance, which is associated with more H_2O_2 accumulation and cell death.

OsCNGC14 and *OsCNGC16* Impact Cytosolic Calcium Increase in Response to Chilling Treatment

To investigate whether *OsCNGC14* and *OsCNGC16* might affect chilling-induced changes in cytosolic Ca^{2+}, we monitored calcium levels in stomatal cells of the wild type and the *cngc* mutants before and after chilling treatment. Chilling triggered a large increase in cytosolic Ca^{2+} in the wild type in 5 s, and subsequent chilling treatments induced very mild Ca^{2+} spikes, with no calcium change observed at the third treatment (Fig. 6, A and B; Supplemental Movie S4). In 17 of the 24 cells observed, the *cngc14-2* mutant displayed a significant decrease in cytosolic Ca^{2+} spike following the first cold treatment, and there was almost no calcium change in any of the 24 cells observed following the second and subsequent chilling treatments (Fig. 6A and C; Supplemental Movie S5). The *cngc16-1* mutant had a stronger defect compared to *cngc14-2* after the chilling treatment. No change in cytosolic Ca^{2+} was observed in the *cngc16-1* mutant after chilling in 19 of 21 cells recorded (Fig. 6, A and D; Supplemental Movie S6). The cytosolic Ca^{2+} levels, measured by maximal changes in FRET signals ($\Delta E_{app}/E_{apprest}$) of YC3.6, were 0.22 ± 0.14 in the wild type, 0.12 ± 0.09 in the *cngc14-2* mutant, and 0.05 ± 0.04 in the *cngc16-1* mutant (Fig. 6, E and F). These results thus indicate that *OsCNGC14* and

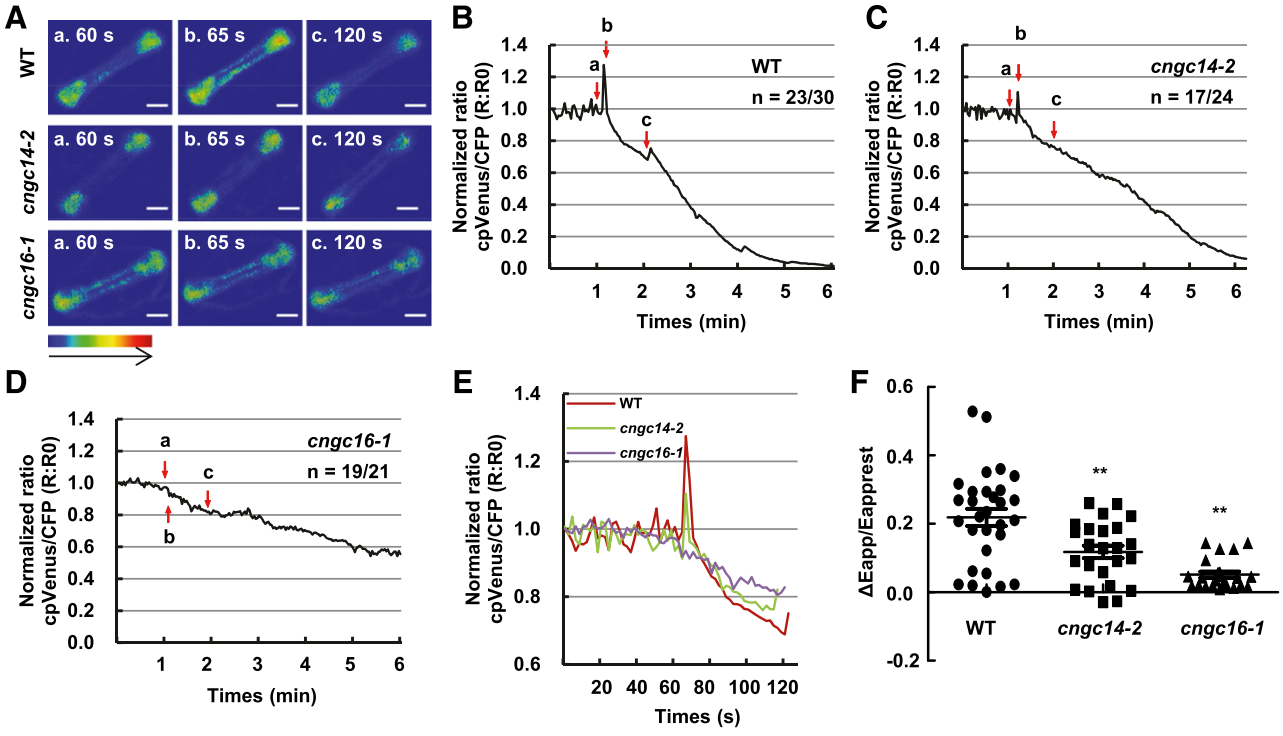

Figure 6. Cold-induced cytosolic Ca^{2+} changes in guard cells of *cngc14* and *cngc16* mutants. A, Emission images of cytosolic Ca^{2+} in the stomatal cells from leaves of wild-type (WT), *cngc14-2*, and *cngc16-1* 10-d-old seedlings expressing NES-YC3.6. Shown are representative images before chilling treatment (60 s) and after chilling treatment (65 and 120 s). The representative image of relative cytosolic Ca^{2+} is represented as the emission fluorescence ratio and scaled by a pseudo-color bar (bottom). Scale bars = 50 μm. B to D, Normalized cytosolic Ca^{2+} FRET ratio in stomatal cells. The luminescence was recorded at 2-s intervals. Shown is the representative image of calcium signals in stomatal cells of the wild type, *cngc14-2*, and *cngc16-1*. Lowercase letters refer to the time points at which these ratio images were taken in A. At least 21 stomatal cells (one leaf/plant, 1–2 stomatal cells/leaf) in the third leaves from at least 10 different seedlings were measured. The two numbers underneath each genotype indicate the number of cells with the representative calcium pattern versus the number of cells analyzed. E, Representative traces of calcium signals from the wild type and the mutants are shown together. F, Scatter plots of the cold-induced changes in cytosolic calcium (Δcytosolic Ca^{2+}) in wild type, *cngc14-2*, and *cngc16-1* as shown in B to D. The Δcytosolic Ca^{2+} indicates the changes between the $[Ca^{2+}]^{peak}$ and $[Ca^{2+}]^{rest}$. Data are from all cells that were monitored (30, 24, and 21 cells for the three genotypes respectively). Asterisks indicate significant difference by Student's *t* test (**$P < 0.01$).

OsCNGC16 are positive modulators of chilling-induced increases in cytosolic Ca^{2+}.

Arabidopsis *AtCNGC2* and *AtCNGC4* Promote Chilling Growth and Freezing Tolerance

Given that the *OsCNGC14* and *OsCNGC16* contribute positively to both heat and chilling tolerance in rice, we asked whether Arabidopsis *AtCNGC2* and *AtCNGC4* affect low-temperature responses in addition to heat tolerance. The Arabidopsis *cngc2* and *cngc4* mutants were assayed for hypocotyl elongation and rosette growth under chilling conditions. The wild-type seedlings displayed shorter hypocotyls when grown at 6°C compared to at 22°C in darkness. The *cngc2* and *cngc4* mutants had shorter hypocotyls but these differences were not statistically significant compared to the wild-type plants at 22°C (Fig. 7, A and B). However, the *cngc2* and *cngc4* mutants displayed significantly shorter hypocotyls compared to wild-type plants at 6°C (Fig. 7, A and B). Chilling (4°C) also inhibited rosette growth in

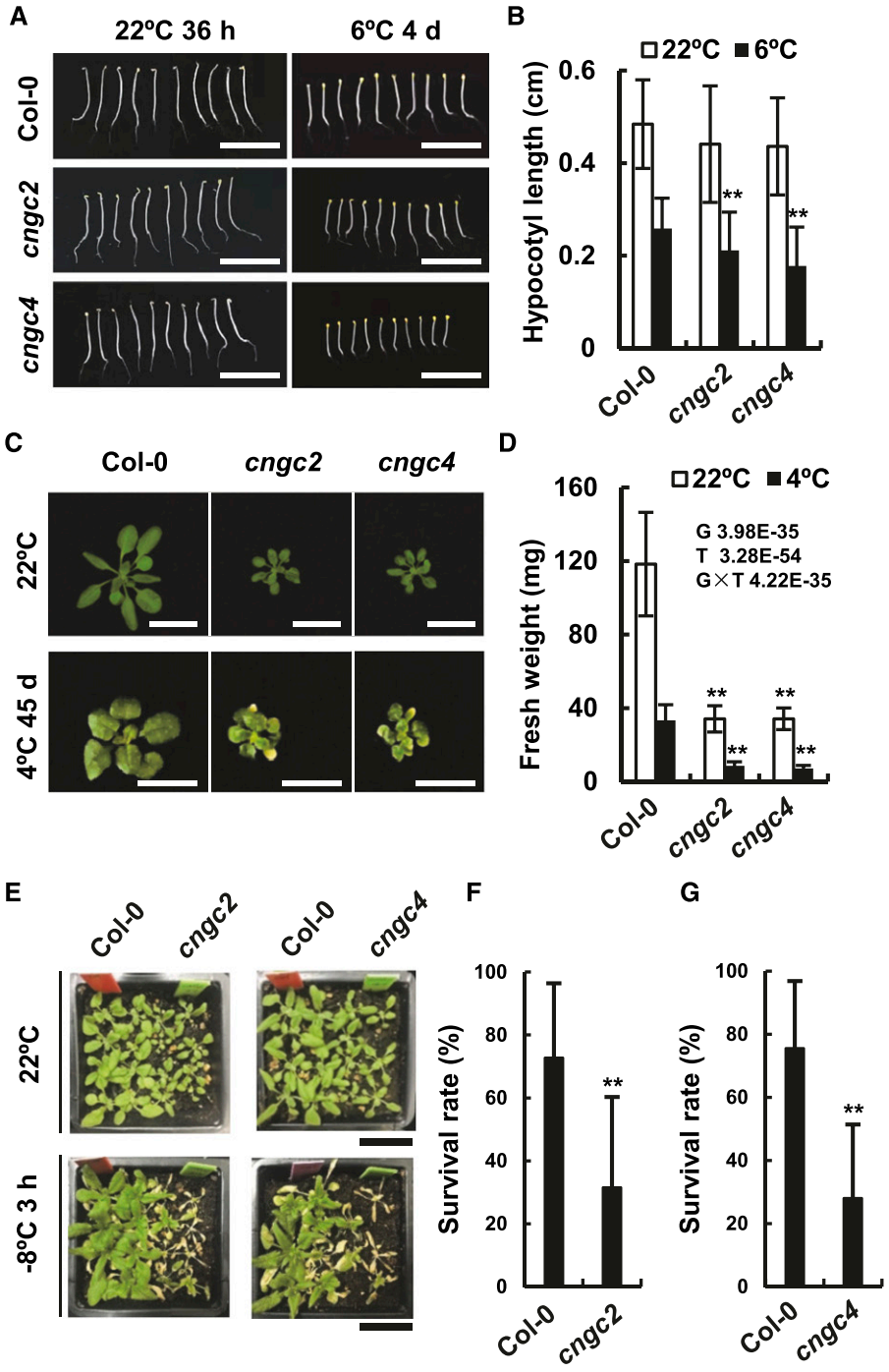

Figure 7. Arabidopsis mutants of *AtCNGC2* and *AtCNGC4* are chilling and freezing susceptible. A and B, Phenotypes (A) and quantification (B) of hypocotyl elongation of *cngc2* and *cngc4* in the dark at 22°C (for 36 h) and 6°C (for 4 d). Data represent means ± SD from three biological replicates, each of which had at least 15 seedlings. C and D, Phenotypes (C) and quantification (D) of rosette growth of the wild type, *cngc2*, and *cngc4* grown on soil at 22°C for 3 weeks and at 6°C for 45 d. Data represent means ± SD from three biological replicates with 10 plants per replica. Double factor variance analysis shows interaction between genotype and temperature. E to G, Phenotypes (E) and survival rate quantifications (F and G) of the wild type and mutants after −8°C treatment for 3 h followed by a 1-week recovery. Data represent means ± SD from nine repeats (one pot per repeat) for each genotype. Asterisks indicate significant difference by Student's *t* test (**$P < 0.01$). Scale bars = 0.5 cm (A), 1 cm (C and D), and 2 cm (E).

the light in the wild type. The fresh weight after 45 d of growth at 4°C was only 30% of that after 21 d of growth at 22°C (Fig. 7, C and D). Both *cngc2* and *cngc4* mutants exhibited more inhibited growth by chilling in the light, with smaller rosettes and reduced fresh weight compared to the wild type when grown at 22°C (Fig. 7C). Compared to the wild type, both mutants had greater reduction in fresh weight (not rosette outgrowth) at 4°C than at 22°C, as indicated by double variant analysis (G × T; Fig. 7D). In addition, both the *cngc2* and *cngc4* mutants exhibited yellow or chlorotic leaves when grown at 4°C, which was not observed in the wild type (Fig. 7C).

We further examined responses to freezing treatments in the Arabidopsis *cngc2* and *cngc4* mutants. When treated at −8°C for 3 h followed by a 1-week recovery period, the *cngc2* mutants displayed a 32% survival rate, significantly lower than the 73% survival rate for the wild-type plants grown side-by-side in the same pot (Fig. 7, E and F). Similarly, the *cngc4* mutants had a 28% survival rate, significantly lower than the 76% rate for the wild type grown in the same pot (Fig. 7, E and G). Taken together, these results indicate that the Arabidopsis *cngc2* and *cngc4* mutants are both impaired in chilling growth and freezing tolerance.

DISCUSSION

Here we report that the rice genes *OsCNGC14* and *OsCNGC16* have critical functions in heat and chilling tolerance. The loss of either *OsCNGC14* or *OsCNGC16* leads to a higher susceptibility to heat and chilling compared to the wild type. In addition, these two rice CNGCs are important for generating cytosolic calcium signals in response to heat and cold, which might further influence transcriptional reprogramming under these stress conditions. Heat tolerance was shown to involve the functions of four Arabidopsis *CNGC* genes (*AtCNGC2*, *AtCNGC4*, *AtCNGC6*, and *AtCNGC 16*) and a moss gene, *PpCNGCb* (Finka et al., 2012; Gao et al., 2012; Tunc-Ozdemir et al., 2013). This study demonstrates that rice CNGCs function in heat-stress tolerance. Moreover, these data provide evidence for a function of plant CNGCs in chilling/freezing tolerance. The Arabidopsis *AtCNGC2* and *AtCNGC4* genes, similar to rice *OsCNGC14* and *OsCNGC16* genes, are required for growth at chilling temperatures and for freezing tolerance. Although the interpretation of this defect could be complicated by the growth defect in the Arabidopsis *cngc2* and *cngc4* mutants, it corroborates a positive role of CNGCs in low-temperature responses observed in rice. Therefore, these findings suggest that the role of CNGCs encompasses a further stress tolerance: chilling and freezing tolerance.

Early studies found a negative impact on heat-stress tolerance from AtCNGC2 and AtCNGC4 in Arabidopsis as well as PpCNGCb in moss (Finka et al., 2012). Here, we find that two of their closest homologs in rice, OsCNGC14 and OsCNGC16, contribute positively to heat tolerance. The first scenario explaining this apparent contradiction is that basal tolerance is assayed in rice and acquired tolerance is assayed in Arabidopsis. A more comprehensive analysis of basal and acquired heat tolerance under different treatment conditions would be needed to compare the roles of Arabidopsis and rice CNGCs. Second, the function of CNGC in heat tolerance could be tissue- or developmental-stage dependent. Consistent with this hypothesis, the *AtCNGC2* gene was found to be a negative regulator of heat tolerance at the seedling stage but a positive regulator of heat tolerance at the reproductive stage (Katano et al., 2018). Third, the loss of CNGC function might generate stress conditions that trigger acclimation when the stress level is above a threshold. It is possible that the extent of stress induced by the loss of *AtCNGC2* or *AtCNGC4* in Arabidopsis might be larger than that induced by the loss of *OsCNGC14* or *OsCNGC16* in rice, and therefore mutations of *AtCNGC2* or *AtCNGC4* in Arabidopsis induce stress acclimation and enhanced heat tolerance. Consistent with this hypothesis, the rice *cngc16* mutant and the wild type had low numbers of DEGs and no enriched GO terms under nonstress conditions, suggesting that the mutant does not significantly up- or downregulate a pathway or process. Nevertheless, in contrast to *AtCNGC2* and *AtCNGC4*, a distantly related gene in Arabidopsis, *AtCNGC6*, was shown to be a positive regulator of acquired heat tolerance (Gao et al., 2012). This indicates that different CNGCs might have different or even opposite impacts on heat tolerance in the same plant.

OsCNGC14 and *OsCNGC16* likely are involved in the early signaling events of both heat and cold responses. Without *OsCNGC14* or *OsCNGC16,* calcium spikes, whether from the first treatment or subsequent treatments of heat or chilling, were reduced in amplitude or totally abolished (Figs. 3 and 6). These results indicate that *OsCNGC14* and *OsCNGC16* are directly or indirectly required for Ca^{2+} influx to the plant cells in response to heat or cold. Similar calcium dynamics in response to heat or chilling have been observed between Arabidopsis and rice (Zheng et al., 2012; Kiegle et al., 2000; Mori et al., 2018; Ma et al., 2015). In Arabidopsis, two Ca^{2+}-permeable mechanosensitive channels, MCA1 and MCA2, were found to mediate chilling-induced calcium influx (Mori et al., 2018). The cold-induced cytosolic Ca^{2+} increase was reduced, but not abolished, in the *mca1 mca2* double mutant, suggesting additional modulators or channels for cold sensing. In rice, *chilling-tolerance divergence1* (*COLD1*), a G-protein signaling regulator, can modulate the activity of the channel protein for calcium influx (Ma et al., 2015). In Arabidopsis, *AtCNGC6*, which mediates the acquisition of thermotolerance, was reported to be required for heat-induced Ca^{2+} influx using the whole-cell patch-clamp technique (Gao et al., 2012). In moss, *PpCNGCb* is also required for calcium influx under heat, although the calcium dynamics after heat is different from that in rice (Finka et al., 2012). The impact of *OsCNGC14* and *OsCNGC16* on calcium signals and

tolerance to heat and chilling makes them candidates for channels responsible for the chilling response. Consistent with a function of *OsCNGC14* or *OsCNGC16* in early temperature-stress signaling, their loss of function or reduction of function led to more signs of stress and damage, such as ROS accumulation, and more cell death in leaves under heat or chilling (Figs. 2, D and E, and 5, D and E). The slightly higher induction of some *HSF* and *HSP* genes in the *cngc16* mutant (Fig. 4C; Supplemental Table S4) also suggests the perception of more severe stress in the mutant after heat treatment.

The study here reveals that the homologous genes *OsCNGC14* and *OsCNGC16* have similar functions in temperature-stress tolerance, but their functions are not redundant or totally overlapping. This indicates that either they function in parallel for maximum responses or they interact to form functional complexes. Complexes of heterodimers or heterotetramers have been observed for CNGCs. In Arabidopsis, a homotetramer of the pollen tube-specific AtCNGC18 is an active Ca^{2+} channel, but the heterotetramer of AtCNGC18 with AtCNGC7 (or AtCNGC8) is inactive (Pan et al., 2019). In rice, OsCNGC15 is very closely related to OsCNGC14 and OsCNGC16 (Supplemental Fig. S1), but a failure to generate its knockout mutant prevented investigation of its function. It will be interesting to examine whether these proteins form complexes among themselves and how complex formation affects their activities in calcium signal generation.

In sum, this study reveals a critical role of CNGCs in low-temperature tolerance as well as in heat tolerance in plants and suggests a shared molecular mechanism in calcium signaling in response to both temperature-stress conditions. Future study should reveal whether and how CNGCs form channels for calcium influx and how they respond to temperature changes and impact temperature-stress signaling.

MATERIALS AND METHODS

Plant Materials and Growth Conditions

The rice genotype used in this study is *Oryza sativa* 'Nipponbare'. Freshly harvested seeds were treated for 2 weeks or more at 42°C to break dormancy, soaked in water at room temperature for 3 to 5 d, and then germinated for 1 d at 37°C. For hydroponic growth, seeds at a similar germination stage were transferred to a 96-well plate (with its bottom cut) sitting in water, as described previously (Huang et al., 2009). Seedlings were grown in chambers with 16 h light at 26°C. For soil growth, germinated seeds were transferred to a mix of vermiculite:special substrate:organic substrate (1:1:1) and cultured at 26°C in the greenhouse.

The Arabidopsis (*Arabidopsis thaliana*) mutants *cngc2* (stock no. CS6523) and *cngc4* (stock no. CS6523) were obtained from the Arabidopsis Biological Resource Center. For Arabidopsis growth, seeds were sown in a mixture of vermiculite:soil (1:1), cold treated at 4°C for 3 d, and germinated and grown in controlled chambers.

Plasmid Constructions and Rice Transformation

For generating CRISPR/Cas9 constructs, specific targets of guide RNA spacer sequences were designed using the CRISPR-PLANT web site (http://www.genome.arizona.edu/crispr/CRISPRsearch.html). Two guide RNA targets were cloned into the PHUE411 construct (Xing et al., 2014) and expressed in cv Nipponbare by *Agrobacterium tumefaciens*-mediated transformation (Nishimura et al., 2006). For subcellular localization, the coding sequences from the genomic DNA were cloned first into the entry vector pDONR221 (Magnani et al., 2006) by BP Clonase II Enzyme mix (Invitrogen) and then into the destination vector phpt-pSATN1-GW (Tzfira et al., 2005) using LR Clonase II Enzyme mix (Invitrogen).

All primer sequences are listed in Supplemental Table S5.

Protein Subcellular Location

Nicotiana benthamiana leaves expressing GFP proteins were analyzed with a ZEISS LSM 780 confocal microscope (ZEISS Microsystems). The excitation lines for imaging GFP and mCherry fusions were 488 and 580 nm, respectively. Images were analyzed using ZEISS Microsystems software.

Heat and Cold Tolerance Assays

Heat and cold tolerance assays were performed using 2-week-old rice plants. Genotypes to be compared were planted side by side each occupying half a plate in the same 96-well plate and treated with 48°C for 48 h (heat) or 6°C for 72 h (chilling). Three plates were treated at the same time and at least three independent treatments were conducted.

Hypocotyl elongation assays were done on seeds sown on one-half strength Murashige and Skoog plates, stratified at 4°C for 3 d, and allowed to germinate at 22°C for 24 h. Seeds at a similar germination stage were then grown at 22°C for 36 h or at 6°C for 4 d in the dark. For measurement of rosette growth under chilling, seedlings were grown first at 22°C for 1 week followed by 45 d at 4°C. Freezing tolerance assays were done on 2-week-old seedlings grown at 22°C in chambers. Plants were moved to a −8°C chamber for 3 h before moving back to the 22°C chamber for 1 week of recovery. Plants of two different genotypes were planted side by side in the same pot for comparison. Nine replicate pots were freezing-stress treated at the same time.

DAB and Trypan Blue Staining

Accumulation of H_2O_2 and cell death were detected by DAB and trypan blue staining, respectively, as described previously (Shen et al., 2015; Thordal-Christensen et al.,1997).

Ion Leakage Analysis

Ion leakage was measured as previously described, with some modifications (Charng et al., 2007). For each sample, three leaves were combined and cut into 0.5-cm pieces and incubated in 0.4 M mannitol at room temperature with gentle shaking for 3 h before the initial conductivity of the solution was measured with a conductivity meter (DDS-307A, Ningbo Hinotek Technology). Total conductivity of the solution was measured after incubation at 85°C for 20 min. The ion leakage rate was expressed as the percentage of initial conductivity divided by total conductivity.

RNA Extraction, RT-PCR, and RT-qPCR

Total RNAs were isolated from seedling tissues using TRIpure Reagent (Bioteke) according to the manufacturer's protocols. One microgram total RNA was reverse transcribed into cDNA using HiScript II RT SuperMix (Vazyme). The cDNAs were then used as templates for qPCR with gene-specific primers. Relative quantitative expression was normalized to the reference gene *OsActin1* (LOC_Os03g61970) and calculated as described previously (Gao et al., 2012). The RT-qPCR was performed using AceQ qPCR SYBR Green Master Mix (Vazyme) and the Bio-Rad CFX96 real-time PCR detection system (Bio-Rad Laboratories). Primer sequences are listed in Supplemental Table S5.

RNA-Seq and Data Analysis

Two-week-old rice seedlings grown in soil at 26°C were heat treated (42°C), and leaf tissues were collected at 0, 3, and 24 h after treatment. Total RNAs were extracted using TRIpure Reagent (Bioteke) according to the manufacturer's protocol. The transcriptomes were sequenced using Illumina HiSeq X Ten (PG150, Illumina). The adaptor sequences and low-quality sequences were removed using Hisat2 (Kim et al., 2015). Approximately 4.7 GB of clean reads

were generated from each sample. The clean reads were mapped to the rice reference genome (IRGSP-1.0). Gene expression normalization among samples was performed using DESeq2 (Love et al., 2014).

PCA analysis was carried out via the web tool https://www.omicshare.com/tools/Home/Soft/pca. The spearman correlation was calculated by the Python Pandas package. Venn diagram analysis was done via the web tool http://bioinfogp.cnb.csic.es/tools/venny/, and the statistical test for overlapping significance was based on the online tool http://nemates.org/MA/progs/overlap_stats.html.

Ca^{2+} Imaging

FRET-based Ca^{2+} imaging was performed as described previously (Li et al., 2017). For heat and cold treatment, images were acquired every 1 and 2 s, respectively.

Statistical Analysis

Data were processed in Excel version 2010 (Microsoft Corporation). Comparisons between group means were performed with Student's *t* test.

Accession Numbers

Sequence data were obtained from the Rice Annotation Project Database (http://rice.plantbiology.msu.edu/index.shtml) according to the following accession numbers: LOC_Os03g55100 (*OsCNGC14*) and LOC_Os05g42250 (*OsCNGC16*). The GenBank accession numbers are as follows: NC_029258.1 (*OsCNGC14*) and NC_029260.1 (*OsCNGC16*).

Supplemental Data

The following supplemental materials are available.

Supplemental Figure S1. Phylogenetic tree of CNGC proteins in Arabidopsis, moss, and rice.

Supplemental Figure S2. Subcellular localization of OsCNGC14 and OsCNGC16.

Supplemental Figure S3. Global expression profiles of *OsCNGC14* and *OsCNGC16* at various stages of development.

Supplemental Figure S4. Expression pattern of *OsCNGC14* and *OsCNGC16* genes in response to heat- and cold-stress conditions.

Supplemental Figure S5. RNA expression of *OsCNGC14* and *OsCNGC16* in the wild type and the *cngc* mutants.

Supplemental Figure S6. Mutants of *OsCNGC14* and *OsCNGC16* are heat and cold susceptible at seedling stage.

Supplemental Figure S7. Signals of NES-YC3.6 in the wild type and the *cngc14* and *cngc16* mutants.

Supplemental Figure S8. Overall analyses of transcriptomes of the wild type and the *cngc16-3* mutant.

Supplemental Figure S9. GO enrichment analysis of DEGs between the *cngc16-3* mutant and the wild type at 3 h and 24 h.

Supplemental Figure S10. Venn diagram showing overlaps of high temperature-responsive genes and DEGs of *cngc16-3* mutant.

Supplemental Table S1. DEGs between *cngc16-3* mutant and the wild type at 0, 3, and 24 h.

Supplemental Table S2. Heat-induced and heat-repressed genes in wild-type plants at 3 and 24 h.

Supplemental Table S3. Heat-induced and heat-repressed genes in the *cngc16-3* mutant at 3 and 24 h.

Supplemental Table S4. Expression levels of *HSF*s and *HSP*s in the wild type and the *cngc16-3* mutant at 0, 3, and 24 h.

Supplemental Table S5. List of primers and their sequences used in this study.

Supplemental Movie S1. Cytosolic Ca^{2+} transient induced in wild-type plants by heat treatment.

Supplemental Movie S2. Cytosolic Ca^{2+} transient induced in *cngc14-2* plants by heat treatment.

Supplemental Movie S3. Cytosolic Ca^{2+} transient induced in *cngc16-1* plants by heat treatment.

Supplemental Movie S4. Cytosolic Ca^{2+} transient induced in wild-type plants by cold treatment.

Supplemental Movie S5. Cytosolic Ca^{2+} transient induced in *cngc14-2* plants by cold treatment.

Supplemental Movie S6. Cytosolic Ca^{2+} transient induced in *cngc16-1* plants by cold treatment.

ACKNOWLEDGMENTS

We thank Dr. Jörg Kudla for the NES-YC3.6 transgenic materials, Qianru Jia and other members of Dr. Wenhua Zhang's group for assisting calcium imaging, and Kejian Shi for assisting in mutant material generation.

Received May 11, 2020; accepted May 29, 2020; published June 11, 2020.

LITERATURE CITED

Atkinson D, Porter JR (1996) Temperature, plant development and crop yields. Trends Plant Sci **1:** 119–124

Behera S, Wang N, Zhang C, Schmitz-Thom I, Strohkamp S, Schültke S, Hashimoto K, Xiong L, Kudla J (2015) Analyses of Ca^{2+} dynamics using a ubiquitin-10 promoter-driven Yellow Cameleon 3.6 indicator reveal reliable transgene expression and differences in cytoplasmic Ca^{2+} responses in Arabidopsis and rice (*Oryza sativa*) roots. New Phytol **206:** 751–760

Borsics T, Webb D, Andeme-Ondzighi C, Staehelin LA, Christopher DA (2007) The cyclic nucleotide-gated calmodulin-binding channel AtCNGC10 localizes to the plasma membrane and influences numerous growth responses and starch accumulation in *Arabidopsis thaliana*. Planta **225:** 563–573

Brost C, Studtrucker T, Reimann R, Denninger P, Czekalla J, Krebs M, Fabry B, Schumacher K, Grossmann G, Dietrich P (2019) Multiple cyclic nucleotide-gated channels coordinate calcium oscillations and polar growth of root hairs. Plant J **99:** 910–923

Chan CWM, Schorrak LM, Smith RKW Jr., Bent AF, Sussman MR (2003) A cyclic nucleotide-gated ion channel, CNGC2, is crucial for plant development and adaptation to calcium stress. Plant Physiol **132:** 728–731

Charng YY, Liu HC, Liu NY, Chi WT, Wang CN, Chang SH, Wang TT (2007) A heat-inducible transcription factor, HsfA2, is required for extension of acquired thermotolerance in Arabidopsis. Plant Physiol **143:** 251–262

Chin K, DeFalco TA, Moeder W, Yoshioka K (2013) The Arabidopsis cyclic nucleotide-gated ion channels AtCNGC2 and AtCNGC4 work in the same signaling pathway to regulate pathogen defense and floral transition. Plant Physiol **163:** 611–624

DeFalco TA, Moeder W, Yoshioka K (2016) Opening the gates: Insights into cyclic nucleotide-gated channel-mediated signaling. Trends Plant Sci **21:** 903–906

Finka A, Cuendet AFH, Maathuis FJM, Saidi Y, Goloubinoff P (2012) Plasma membrane cyclic nucleotide gated calcium channels control land plant thermal sensing and acquired thermotolerance. Plant Cell **24:** 3333–3348

Fragkostefanakis S, Mesihovic A, Hu Y, Schleiff E (2016) Unfolded protein response in pollen development and heat stress tolerance. Plant Reprod **29:** 81–91

Gao F, Han X, Wu J, Zheng S, Shang Z, Sun D, Zhou R, Li B (2012) A heat-activated calcium-permeable channel—Arabidopsis cyclic nucleotide-gated ion channel 6—is involved in heat shock responses. Plant J **70:** 1056–1069

Gobert A, Park G, Amtmann A, Sanders D, Maathuis FJM (2006) *Arabidopsis thaliana* cyclic nucleotide gated channel 3 forms a non-selective ion

transporter involved in germination and cation transport. J Exp Bot **57:** 791–800

Guo KM, Babourina O, Christopher DA, Borsics T, Rengel Z (2008) The cyclic nucleotide-gated channel, AtCNGC10, influences salt tolerance in *Arabidopsis*. Physiol Plant **134:** 499–507

Hatfield JL, Prueger JH (2015) Temperature extremes: Effect on plant growth and development. Weather Clim Extrem **10:** 4–10

Huang XY, Chao DY, Gao JP, Zhu MZ, Shi M, Lin HX (2009) A previously unknown zinc finger protein, DST, regulates drought and salt tolerance in rice via stomatal aperture control. Genes Dev **23:** 1805–1817

Katano K, Kataoka R, Fujii M, Suzuki N (2018) Differences between seedlings and flowers in anti-ROS based heat responses of Arabidopsis plants deficient in cyclic nucleotide gated channel 2. Plant Physiol Biochem **123:** 288–296

Kiegle E, Moore CA, Haseloff J, Tester MA, Knight MR (2000) Cell-type-specific calcium responses to drought, salt and cold in the Arabidopsis root. Plant J **23:** 267–278

Kim D, Langmead B, Salzberg SL (2015) HISAT: A fast spliced aligner with low memory requirements. Nat Methods **12:** 357–360

Krebs M, Held K, Binder A, Hashimoto K, Den Herder G, Parniske M, Kudla J, Schumacher K (2012) FRET-based genetically encoded sensors allow high-resolution live cell imaging of Ca^{2+} dynamics. Plant J **69:** 181–192

Kugler A, Köhler B, Palme K, Wolff P, Dietrich P (2009) Salt-dependent regulation of a CNG channel subfamily in Arabidopsis. BMC Plant Biol **9:** 140–150

Ladwig F, Dahlke RI, Stührwohldt N, Hartmann J, Harter K, Sauter M (2015) Phytosulfokine regulates growth in Arabidopsis through a response module at the plasma membrane that includes CYCLIC NUCLEOTIDE-GATED CHANNEL17, H^+-ATPase, and BAK1. Plant Cell **27:** 1718–1729

Leeggangers HACF, Nijveen H, Bigas JN, Hilhorst HWM, Immink RGH (2017) Molecular regulation of temperature-dependent floral induction in *Tulipa gesneriana*. Plant Physiol **173:** 1904–1919

Li L, Wang F, Yan P, Jing W, Zhang C, Kudla J, Zhang W (2017) A phosphoinositide-specific phospholipase C pathway elicits stress-induced Ca^{2+} signals and confers salt tolerance to rice. New Phytol **214:** 1172–1187

Liu HT, Gao F, Li GL, Han JL, Liu DL, Sun DY, Zhou RG (2008) The calmodulin-binding protein kinase 3 is part of heat-shock signal transduction in *Arabidopsis thaliana*. Plant J **55:** 760–773

Liu HT, Li B, Shang ZL, Li XZ, Mu RL, Sun DY, Zhou RG (2003) Calmodulin is involved in heat shock signal transduction in wheat. Plant Physiol **132:** 1186–1195

Liu J, Niu Y, Zhang J, Zhou Y, Ma Z, Huang X (2018) Ca^{2+} channels and Ca^{2+} signals involved in abiotic stress responses in plant cells: Recent advances. Plant Cell Tissue Organ Cult **132:** 413–424

Liu J, Zhang C, Wei C, Liu X, Wang M, Yu F, Xie Q, Tu J (2016) The RING finger ubiquitin E3 ligase OsHTAS enhances heat tolerance by promoting H_2O_2-induced stomatal closure in rice. Plant Physiol **170:** 429–443

Liu Q, Kasuga M, Sakuma Y, Abe H, Miura S, Yamaguchi-Shinozaki K, Shinozaki K (1998) Two transcription factors, DREB1 and DREB2, with an EREBP/AP2 DNA binding domain separate two cellular signal transduction pathways in drought- and low-temperature-responsive gene expression, respectively, in *Arabidopsis*. Plant Cell **10:** 1391–1406

Love MI, Huber W, Anders S (2014) Moderated estimation of fold change and dispersion for RNA-seq with DESeq2. Genome Biol **15:** 550

Ma W, Ali R, Berkowitz GA (2006) Characterization of plant phenotypes associated with loss-of-function of AtCNGC1, a plant cyclic nucleotide gated cation channel. Plant Physiol Biochem **44:** 494–505

Ma Y, Dai X, Xu Y, Luo W, Zheng X, Zeng D, Pan Y, Lin X, Liu H, Zhang D, et al (2015) COLD1 confers chilling tolerance in rice. Cell **160:** 1209–1221

Magnani E, Bartling L, Hake S (2006) From Gateway to MultiSite Gateway in one recombination event. BMC Mol Biol **7:** 46

Meena MK, Prajapati R, Krishna D, Divakaran K, Pandey Y, Reichelt M, Mathew MK, Boland W, Mithöfer A, Vadassery J (2019) The Ca^{2+} channel CNGC19 regulates Arabidopsis defense against Spodoptera herbivory. Plant Cell **31:** 1539–1562

Mittler R (2002) Oxidative stress, antioxidants and stress tolerance. Trends Plant Sci **7:** 405–410

Mori K, Renhu N, Naito M, Nakamura A, Shiba H, Yamamoto T, Suzaki T, Iida H, Miura K (2018) Ca^{2+}-permeable mechanosensitive channels MCA1 and MCA2 mediate cold-induced cytosolic Ca^{2+} increase and cold tolerance in Arabidopsis. Sci Rep **8:** 550

Murakami Y, Tsuyama M, Kobayashi Y, Kodama H, Iba K (2000) Trienoic fatty acids and plant tolerance of high temperature. Science **287:** 476–479

Murata N, Los DA (1997) Membrane fluidity and temperature perception. Plant Physiol **115:** 875–879

Nawaz Z, Kakar KU, Saand MA, Shu Q-Y (2014) Cyclic nucleotide-gated ion channel gene family in rice, identification, characterization and experimental analysis of expression response to plant hormones, biotic and abiotic stresses. BMC Genomics **15:** 853–860

Nguyen AN, Shiozaki K (1999) Heat-shock-induced activation of stress MAP kinase is regulated by threonine- and tyrosine-specific phosphatases. Genes Dev **13:** 1653–1663

Nishimura A, Aichi I, Matsuoka M (2006) A protocol for *Agrobacterium*-mediated transformation in rice. Nat Protoc **1:** 2796–2802

Ohama N, Sato H, Shinozaki K, Yamaguchi-Shinozaki K (2017) Transcriptional regulatory network of plant heat stress response. Trends Plant Sci **22:** 53–65

Pan Y, Chai X, Gao Q, Zhou L, Zhang S, Li L, Luan S (2019) Dynamic interactions of plant CNGC subunits and calmodulins drive oscillatory Ca^{2+} channel activities. Dev Cell **48:** 710–725.e5

Prasad TK, Anderson MD, Martin BA, Stewart CR (1994) Evidence for chilling-induced oxidative stress in maize seedlings and a regulatory role for hydrogen peroxide. Plant Cell **6:** 65–74

Rieu I, Twell D, Firon N (2017) Pollen development at high temperature: From acclimation to collapse. Plant Physiol **173:** 1967–1976

Saidi Y, Finka A, Goloubinoff P (2011) Heat perception and signalling in plants: A tortuous path to thermotolerance. New Phytol **190:** 556–565

Saidi Y, Finka A, Muriset M, Bromberg Z, Weiss YG, Maathuis FJM, Goloubinoff P (2009) The heat shock response in moss plants is regulated by specific calcium-permeable channels in the plasma membrane. Plant Cell **21:** 2829–2843

Shen H, Zhong X, Zhao F, Wang Y, Yan B, Li Q, Chen G, Mao B, Wang J, Li Y, et al (2015) Overexpression of receptor-like kinase *ERECTA* improves thermotolerance in rice and tomato. Nat Biotechnol **33:** 996–1003

Stockinger EJ, Gilmour SJ, Thomashow MF (1997) *Arabidopsis thaliana* CBF1 encodes an AP2 domain-containing transcriptional activator that binds to the C-repeat/DRE, a cis-acting DNA regulatory element that stimulates transcription in response to low temperature and water deficit. Proc Natl Acad Sci USA **94:** 1035–1040

Tan Y-Q, Yang Y, Zhang A, Fei C-F, Gu L-L, Sun S-J, Xu W, Wang L, Liu H, Wang Y-F (2019) Three CNGC family members, CNGC5, CNGC6, and CNGC9, are required for constitutive growth of *Arabidopsis* root hairs as Ca^{2+}-permeable channels. Plant Commun **1:** 100001

Thordal-Christensen H, Zhang Z, Wei YD, Collinge DB (1997) Subcellular localization of H_2O_2 in plants. H_2O_2 accumulation in papillae and hypersensitive response during the barley-powdery mildew interaction. Plant J **11:** 1187–1194

Tunc-Ozdemir M, Tang C, Ishka MR, Brown E, Groves NR, Myers CT, Rato C, Poulsen LR, McDowell S, Miller G, et al (2013) A cyclic nucleotide-gated channel (CNGC16) in pollen is critical for stress tolerance in pollen reproductive development. Plant Physiol **161:** 1010–1020

Tzfira T, Tian GW, Lacroix B, Vyas S, Li J, Leitner-Dagan Y, Krichevsky A, Taylor T, Vainstein A, Citovsky V (2005) pSAT vectors: A modular series of plasmids for autofluorescent protein tagging and expression of multiple genes in plants. Plant Mol Biol **57:** 503–516

Wada H, Gombos Z, Murata N (1990) Enhancement of chilling tolerance of a cyanobacterium by genetic manipulation of fatty acid desaturation. Nature **347:** 200–203

Wang J, Liu X, Zhang A, Ren Y, Wu F, Wang G, Xu Y, Lei C, Zhu S, Pan T, et al (2019) A cyclic nucleotide-gated channel mediates cytoplasmic calcium elevation and disease resistance in rice. Cell Res **29:** 820–831

Wang Y, Kang Y, Ma C, Miao R, Wu C, Long Y, Ge T, Wu Z, Hou X, Zhang J, et al (2017) CNGC2 is a Ca^{2+} influx channel that prevents accumulation of apoplastic Ca^{2+} in the leaf. Plant Physiol **173:** 1342–1354

Xing HL, Dong L, Wang ZP, Zhang HY, Han CY, Liu B, Wang XC, Chen QJ (2014) A CRISPR/Cas9 toolkit for multiplex genome editing in plants. BMC Plant Biol **14:** 327

Xu Y, Yang J, Wang Y, Wang J, Yu Y, Long Y, Wang Y, Zhang H, Ren Y, Chen J, et al (2017) OsCNGC13 promotes seed-setting rate by facilitating pollen tube growth in stylar tissues. PLoS Genet **13:** e1006906

Yan Y, Wei CL, Zhang WR, Cheng HP, Liu J (2006) Cross-talk between calcium and reactive oxygen species signaling. Acta Pharmacol Sin **27:** 821–826

Yoshioka K, Moeder W, Kang HG, Kachroo P, Masmoudi K, Berkowitz G, Klessig DF (2006) The chimeric *Arabidopsis* CYCLIC NUCLEOTIDE-GATED ION CHANNEL11/12 activates multiple pathogen resistance responses. Plant Cell **18:** 747–763

Zhang J, Li XM, Lin HX, Chong K (2019) Crop improvement through temperature resilience. Annu Rev Plant Biol **70:** 753–780

Zhang Z, Li J, Li F, Liu H, Yang W, Chong K, Xu Y (2017) OsMAPK3 phosphorylates OsbHLH002/OsICE1 and inhibits its ubiquitination to activate *OsTPP1* and enhances rice chilling tolerance. Dev Cell **43:** 731–743.e5

Zheng SZ, Liu YL, Li B, Shang ZL, Zhou RG, Sun DY (2012) Phosphoinositide-specific phospholipase C9 is involved in the thermotolerance of Arabidopsis. Plant J **69:** 689–700